Atmos. Chem. Phys. Discuss., 9, 12559–12596, 2009
www.atmos-chem-phys-discuss.net/9/12559/2009/

Atmospheric Chemistry and Physics Discussions

This discussion paper is/has been under review for the journal *Atmospheric Chemistry and Physics (ACP)*. Please refer to the corresponding final paper in *ACP* if available.

Photolytic control of the nitrate stable isotope signal in snow and atmosphere of East Antarctica and implications for reactive nitrogen cycling

M. M. Frey[1,2,*], **J. Savarino**[1,2], **S. Morin**[1,2], **J. Erbland**[1,2], **and J. M. F. Martins**[1,3]

[1]CNRS – Institut National des Sciences de l'Univers (INSU), France
[2]Laboratoire de Glaciologie et Géophysique de l'Environnement, Université Joseph Fourier-Grenoble, St Martin d'Hères, France
[3]Laboratoire d'Etude de Transferts en Hydrologie et Environnement, Université Joseph Fourier-Grenoble, St Martin d'Hères, France
[*]now at: British Antarctic Survey, Natural Environment Research Council, Cambridge, United Kingdom

Received: 3 May 2009 – Accepted: 12 May 2009 – Published: 27 May 2009

Correspondence to: M. M. Frey (maey@bas.ac.uk)

Published by Copernicus Publications on behalf of the European Geosciences Union.

Abstract

The nitrogen ($\delta^{15}N$) and triple oxygen ($\delta^{17/18}O$) isotopic composition of nitrate (NO_3^-) was measured year-round in the atmosphere and snow pits at Dome C (DC, 75.1° S, 123.3° E), and in surface snow on a transect between DC and the coast. Snow pit profiles of $\delta^{15}N$ ($\delta^{18}O$) in NO_3^- show significant enrichment (depletion) of >200 (<40) ‰ compared to the isotopic signal in atmospheric NO_3^-, whereas post-depositional fractionation in $\Delta^{17}O(NO_3^-)$ is small, allowing reconstruction of past shifts in tropospheric oxidation pathways from ice cores. Assuming a Rayleigh-type process we find in the DC04 (DC07) pit fractionation factors ε of −50±10 (−71±12) ‰, 6±3 (9±2) ‰ and 1±0.2 (2±0.6) ‰, for $\delta^{15}N$, $\delta^{18}O$ and $\Delta^{17}O$, respectively. A photolysis model reproduces ε for $\delta^{15}N$ within the range of uncertainty at DC and for lab experiments reported by Blunier et al. (2005), suggesting that the current literature value for photolytic isotopic fractionation in snow is significantly underestimated. Depletion of oxygen stable isotopes is attributed to photolysis followed by isotopic exchange with water and hydroxyl radicals. Conversely, ^{15}N enrichment of the NO_3^- fraction in the snow implies ^{15}N depletion of emissions. Indeed, $\delta^{15}N$ in atmospheric NO_3^- shows a strong decrease from background levels (4.4±6.8‰) to −35.1‰ in spring followed by recovery during summer, consistent with significant snow pack emissions of reactive nitrogen. Field and lab evidence therefore suggest that photolysis dominates fractionation and associated NO_3^- loss from snow in the low-accumulation regions of the East Antarctic Ice Sheet (EAIS). The $\Delta^{17}O$ signature confirms previous coastal measurements that the peak of atmospheric NO_3^- in spring is of stratospheric origin. After sunrise photolysis drives then redistribution of NO_3^- from the snowpack photic zone to the atmosphere and a snow surface skin layer, thereby concentrating NO_3^- at the surface. Little NO_3^- is exported off the EAIS plateau, still snow emissions from as far as 600 km inland can contribute to the coastal NO_3^- budget.

ACPD

9, 12559–12596, 2009

1 Introduction

Nitrate (NO_3^-) is the chemical species at the end of the oxidation chain of atmospheric reactive nitrogen and is one of the dominant anions present in the polar snow pack (Legrand et al., 1999). Therefore there has been vital interest in using the polar ice core record of NO_3^- concentrations to reconstruct past levels of atmospheric nitrogen oxides (NO_x=NO+NO_2) and rates of stratospheric denitrification (Mulvaney and Wolff, 1993; Wolff and Delmas, 1995). Recent studies in the Arctic and Antarctic suggested furthermore that the stable isotopic composition of NO_3^- in snow has great potential in providing constraints on NO_3^- sources and NO_x oxidation pathways (Hastings et al., 2004; McCabe et al., 2007; Savarino et al., 2007; Kunasek et al., 2008; Morin et al., 2008, 2009).

However, post-depositional processing of NO_3^- leads to significant mass loss and isotopic fractionation, especially at sites with low annual accumulation rates, and compromises a quantitative atmospheric interpretation of the ice core record (Mulvaney et al., 1998; Röthlisberger et al., 2002; Wolff et al., 2008; Blunier et al., 2005). Recently, the same NO_3^- loss from snow was related to re-emission of oxidized nitrogen species into the lower atmosphere above snow covered areas with a significant impact on tropospheric oxidant chemistry, a discovery which triggered a suite of field and lab studies (Grannas et al., 2007, and references therein). Post-depositional mass loss and isotopic fractionation at sites of intermediate annual accumulation rates may be less important (Hastings et al., 2004; Jarvis et al., 2008). However, a quantitative understanding of the nature of post-depositional processes affecting NO_3^- in snow is urgently needed in order to a) to use the ice core record to reconstruct past atmospheric composition and b) better understand current boundary layer chemistry above snow surfaces.

Both photochemical and physical processes in the upper snow pack drive the observed net loss of NO_3^- (Röthlisberger et al., 2002), but relative contributions from UV-photolysis of NO_3^- and evaporation of nitric acid (HNO_3) are still under debate. Model

ACPD
9, 12559–12596, 2009

studies have shown that NO_3^- photolysis on and in snow/ice surfaces can account for observed volumetric fluxes and concentrations of NO and NO_2 above the Arctic and coastal Antarctic snow pack (Wolff et al., 2002; Boxe and Saiz-Lopez, 2008). But according to one model only up to 40% of NO_3^- loss from the snow reservoir can be achieved by photolysis (Wolff et al., 2002). A recent isotopic study on Antarctic snow compared field and lab determined fractionation constants of the stable nitrogen isotope in NO_3^- and concluded that photolysis is not the main process leading to NO_3^- loss at the snow surface (Blunier et al., 2005).

The following simplified reaction scheme summarizes currently known NO_3^- photochemistry in snow:

$$NO_3^- + h\nu \rightarrow NO_2 + O^- \quad \text{(R1)}$$

$$NO_3^- + h\nu \rightarrow NO_2^- + O(^3P) \quad \text{(R2)}$$

$$NO_2^- + h\nu \rightarrow NO + O^- \quad \text{(R3)}$$

$$NO_2^- + OH \rightarrow NO_2 + OH^- \quad \text{(R4)}$$

At surface relevant wavelengths (>290 nm) NO_3^- photolyses in an absorption band centered around 302 nm (Chu and Anastasio, 2003) yielding NO_2 (Reaction R1) and nitrite (NO_2^-) (Reaction R2). NO_2^- undergoes either photolysis with UV-absorption maxima around 318 nm and 354 nm (Reaction R3) or reacts with the hydroxyl radical (OH) (Reaction R4) to produce NO and NO_2, respectively (Boxe and Saiz-Lopez, 2008). The oxide radical ion (O^-) produced in Reactions (R1) and (R3) are immediately protonated contributing to the OH photo formation in snow (Anastasio et al., 2007). In addition, nitrous acid (HONO) is formed at pH<7.

$$NO_2^- + H^+ \rightarrow HONO \quad \text{(R5)}$$

Since Reaction (R1) exceeds Reaction (R2) by a factor 8 to 9 the dominant NO_3^- photolysis product is NO_2 followed by NO and HONO (Grannas et al., 2007).

ACPD
9, 12559–12596, 2009

In this study we compare for the first time measurements of the stable isotopes of oxygen and nitrogen in NO_3^- from snow pits with year-round observations in atmospheric NO_3^- at Dome Concordia (from here on DC, 75.1° S, 123.3° E, 3233 m.a.m.s.l.). Snow samples from a spatial survey on the East Antarctic ice sheet (EAIS) were also included. The purpose is (a) to evaluate post-depositional isotopic fractionation to determine the main process driving NO_3^- loss from snow and (b) to discuss implications for reactive nitrogen cycling above Antarctica and the interpretation of the ice core record of NO_3^- stable isotopes.

2 Methods

Snow pits of 6 m and 0.5 m depth were sampled at DC on 15 January 2004 and 18 December 2007 at 2–5 cm depth resolution. For the purpose of investigating post-depositional isotopic fractionation we discuss only surface-near measurements from the top 0.7 m and will present the interpretation of the full DC04 profile in a future manuscript. Samples were collected also from the top 10 cm of snow pack on the logistical ground traverse returning from DC to the french coastal station Dumont d'Urville (from here on DDU, 66.7° S, 140.0° E, 40 m.a.m.s.l.), in January 2004 (Fig. 2). Surface snow samples represent between 1 (coast) and 13 (plateau) months of past net accumulation due to the strong spatial gradient in precipitation (Pettre et al., 1986). Note that sample sizes ranged from 0.3 kg in 2007 to 3 kg in 2004.

In order to obtain 100 nmol of NO_3^- for isotopic analysis snow samples were melted and preconcentrated after Silva et al. (2000). This involved quantitative trapping of NO_3^- on 0.2 ml of anion exchange resin (BioRad AG 1-X8) with an exchange capacity of 1.2 meq ml^{-1}, followed by elution with 5×2 ml of NaCl solution (1M) yielding 100% mass recovery within the analytical uncertainty. The 2004 snow samples were shipped frozen in double-sealed plastic bags to a commercial freezer storage facility in France, whereas 2007 samples were preconcentrated in the warm lab at DC before shipping of refrozen aliquots. NO_3^- concentrations were determined using a colorimetric method

ACPD
9, 12559–12596, 2009

applied on a routine basis in continuous flow analysis of polar ice cores with a detection limit of 0.5 ng g^{-1} and precision of <3% (e.g. Frey et al., 2006). Atmospheric NO_3^- was collected at DC between January 2007 and January 2008 at 2-weekly resolution using a high-volume air sampler (Thermo Andersen GL 2000H) at 1.0 STP–m^3 min^{-1}, following a similar experimental procedure as described in Savarino et al. (2007). The atmospheric NO_3^- collected on glass fiber filters represents the sum of atmospheric particulate NO_3^- (p-NO_3^-) and gaseous nitric acid (HNO_3). This method did not allow to separate the two components of atmospheric NO_3^-, since HNO_3 readily adsorbs to aerosols on the filters and second-stage filters showed either very low NO_3^- concentrations or none at all. After sample collection filters were stored frozen in clean 50 ml-centrifuge tubes, before shipment to France. In our laboratory the collected NO_3^- was transferred quantitatively into solution by centrifuging the filters in 40 ml of ultra-pure water.

We used the denitrifier method developed by Sigman et al. (2001) and Casciotti et al. (2002) and further improved by Kaiser et al. (2007) to determine the nitrogen and triple oxygen isotopic composition of NO_3^- (further details in Morin et al., 2008, 2009). In brief, sample NO_3^- was quantitatively reduced into nitrous oxide (N_2O) during over-night incubation in concentrated solutions of *Pseudomonas aureofaciens*. We employed an on-line method, where the N_2O purged from the sample vials was decomposed on a gold furnace at 900°C into O_2 and N_2 followed by gas chromatographic separation and injection into an Isotope Ratio Mass Spectrometer (IRMS) (Thermo Finnigan MAT 253). The oxygen isotope ratios were referenced against Vienna Standard Mean Ocean Water (VSMOW) (Baertschi, 1976; Li et al., 1988), whereas $^{15}N/^{14}N$ was measured against AIR (Mariotti, 1983). All isotopic measurements were corrected using the international reference materials USGS 32, USGS 34 and USGS 35, which are anchored to the VSMOW (AIR) reference for oxygen (nitrogen) isotopes (Böhlke et al., 2003). The isotope ratios $^{17}O/^{16}O$, $^{18}O/^{16}O$ and $^{15}N/^{14}N$ of NO_3^- are reported as δ-values, where $\delta=(R_{spl}/R_{std}-1)$, with R being the elemental isotope ratios in sample and standard, respectively. The oxygen isotope anomaly of NO_3^- is here defined

by its linear approximation as $\Delta^{17}O = \delta^{17}O - 0.52 \times \delta^{18}O$. The overall accuracy of the method was calculated as the best estimate for the standard deviation of the residuals from a linear regression between measured standards and their expected values (after Taylor, 1997, p. 187). Reported snow samples have average accuracies of 1.3, 0.6 and 0.4‰ and filter samples of 1.4, 0.3 and 0.7‰ for $\delta^{18}O$, $\Delta^{17}O$, and $\delta^{15}N$, respectively.

3 Results

3.1 Snow NO_3^-

NO_3^- concentrations drop in both snow pits within the top 50 cm to less than 10% of surface levels ranging from 240 to 325 ng g^{-1} (Fig. 1c). $\delta^{15}N(NO_3^-)$ values increase by >200‰ whereas $\delta^{18}O(NO_3^-)$ levels decrease by 20–40‰ within the top 70 cm resulting in a statistically significant anti-correlation between the two isotopes ($r = -0.9$, $p < 0.001$) (Fig. 1b, c). The $\Delta^{17}O(NO_3^-)$ profile exhibits periodic oscillations with an amplitude of 4–5‰ (Fig. 1a), found also in two additional snow pits (Frey et al., 2009). Comparison of the top and bottom values of $\Delta^{17}O(NO_3^-)$ in both snow pits reveals a decreasing trend of more than 4‰, from 28 to 24‰ in 2004 and from 32 to 27‰ in 2007 (Fig. 1a).

NO_3^- concentrations in surface snow between DC and DDU range from 112 to 435 ng g^{-1}, with maxima occurring on the East Antarctic plateau (Fig. 2). $\delta^{15}N(NO_3^-)$ varies between −13 and 37‰, and shows a strong spatial gradient from negative values below 2700 m.a.m.s.l. (−8 to −4‰) to positive isotope ratios on the plateau above 3000 m.a.m.s.l. (22–34‰), with a transition zone of high variability (Fig. 2a). $\delta^{18}O(NO_3^-)$ exhibits also a spatial gradient but weaker and of opposite sign, with low isotope ratios on the East Antarctic plateau of <65‰ and high levels of >75‰ towards the coast (Fig. 2b). However, the spatial correlation between the two isotopic ratios is not significant ($r = -0.4$, $p < 0.2$). The average $\pm 1\sigma$ of $\Delta^{17}O(NO_3^-)$ is 30 ± 3 and no significant spatial trend is detected (data not shown).

ACPD
9, 12559–12596, 2009

3.2 Atmospheric NO_3^-

Average ($\pm 1\sigma$) levels in atmospheric NO_3^- between February and July 2007 are 4.5($\pm$3.8) ng m^{-3}, with local maxima in late winter (August–September) of 50 ng m^{-3} and in summer (December–January) of 142 ng m^{-3}, very similar to the coastal record at DDU in 2001 (Savarino et al., 2007) (Fig. 3b). The annual cycles of $\delta^{18}O(NO_3^-)$ and $\Delta^{17}O(NO_3^-)$ compare well to those observed at DDU and South Pole (McCabe et al., 2007; Savarino et al., 2007), showing broad maxima in late winter and early spring of >100‰ and >40‰, respectively (Fig. 3d, e). The annual variability of $\delta^{15}N(NO_3^-)$ features moderate oscillations between −7 and 13‰ around a February–July mean of 4‰ but interrupted by a gradual decrease starting at the end of August as surface temperatures and UV-B radiation begin to rise, reaching strongly negative values with a minimum of −35‰ in mid-October, followed by a recovery to the February–July average by December (Fig. 3a, c). While April-October levels are almost indistinguishable between DC in 2007 and DDU in 2001 and similar to those at Neumayer station observed during the 1986–1992 period (Wagenbach et al., 1998), coastal $\delta^{15}N(NO_3^-)$ remains negative throughout the summer months and no recovery occurs as seen at DC (Fig. 3c).

4 Discussion

4.1 Post-depositional isotopic fractionation

The DC07 NO_3^- snow profile is similar to those published previously, showing >90% NO_3^- loss in the top 10 cm (Röthlisberger et al., 2000; Blunier et al., 2005), whereas in 2004 NO_3^- concentrations exhibit a more gradual decline with depth (Fig. 1c). Spatial variability in concentration profiles has been noted in on-going surface studies at DC and is attributed to sastrugi formation and wind drift in the vicinity of the station (Frey et

al., 2009). Regardless of the NO_3^- profile, trends with depth of NO_3^- stable isotopes are similar in pits sampled in different years (Fig. 1). Some of the most extreme $\delta^{15}N(NO_3^-)$ values found so far in polar snow and ice are observed, exceeding the −18 to 200‰ range previously reported (Freyer et al., 1996; Heaton et al., 2004; Hastings et al., 2004; Blunier et al., 2005). $\delta^{18}O(NO_3^-)$ in surface snow from pit and spatial survey samples ranges between 55 and 85‰ and thus overlaps with measurements in the high Arctic and Greenland (Heaton et al., 2004; Hastings et al., 2004), but drops at depth to values below 30‰ (Figs. 1b, 2b). $\Delta^{17}O(NO_3^-)$ values in snow pit and spatial survey samples vary between 24 and 36‰ (Fig. 1a), a range similar to measurements in snow pits from South Pole and Summit, Greenland (McCabe et al., 2007; Kunasek et al., 2008).

Most importantly, profiles of $\delta^{15}N$ ($\delta^{18}O$) in NO_3^- in snow are strongly enriched (depleted) compared to the isotopic signal registered in atmospheric NO_3^-. The isotopic atmospheric input above the Antarctic ice sheet shows spatial but no temporal variability during the past decade (Fig. 3c–e) and pit profiles of the top 0.7 m of snow, equivalent to about 10 yr, sampled in different years overlap (Fig. 1). From this we conclude that post–depositional isotopic fractionation and not atmospheric trends control $\delta^{15}N$ and $\delta^{18}O$ in NO_3^- at low-accumulation sites such as DC, leading to reproducible profiles as long as the boundary conditions remain unchanged. In the case of $\Delta^{17}O(NO_3^-)$ post-depositional fractionation is significant, e.g. loss of the winter/spring maximum of >40‰ in atmospheric NO_3^- (Fig. 3e), but less severe across the top 0.7m (Fig. 1a). Although post-depositional effects in the upper snow pack erase any seasonal signal in NO_3^- concentrations and isotopic composition (Figs. 1, 3), we still find an oscillation in $\Delta^{17}O(NO_3^-)$ with a mean periodicity of 2.3–3.0 yr based on the range of published accumulation rates of 2.7–3.5 g cm^{-2} yr^{-1} (Legrand and Delmas, 1988; Röthlisberger et al., 2000) (Fig. 1a). A similar 2.7 yr cycle in $\Delta^{17}O(NO_3^-)$ has been detected previously in a 26-yr snow pit record at South Pole, where accumulation rate is 8±3 g cm^{-2} yr^{-1}, almost three times that at DC (e.g. Frey et al., 2006), and was speculated to be linked

ACPD
9, 12559–12596, 2009

to stratospheric ozone variability (McCabe et al., 2007).

In order to compare between sites and lab experiments we estimate bulk fractionation factors ε based on a Rayleigh–type process as described previously (Fig. 4, Table 1, Blunier et al., 2005). The model assumes that NO_3^- loss from the snow is irreversible and emitted mass fractions are removed immediately. For clarity we repeat here the equations used by Blunier et al. (2005). The isotope ratio (δ value) of the NO_3^- mass fraction f remaining in the snow R_{snow} (δ_{snow}) is related to the initial isotope ratio $R_{0,snow}$ ($\delta_{0,snow}$) with $\varepsilon=(\alpha\text{-}1)$ as the fractionation factor through the following relationship:

$$\frac{R_{snow}}{R_{0,snow}} = \frac{\delta_{snow} + 1}{\delta_{0,snow} + 1} = f^{(\alpha\text{-}1)} \quad (1)$$

Regrouping and substitution of $f = c_{snow}/c_{0,snow}$, where $c_{0,snow}$ is the initial surface snow concentration and c_{snow} the concentration of fraction f remaining in the snow, lead to expressions, which allow to estimate ε using a linear regression:

$$ln(\delta_{snow} + 1) = (\alpha\text{-}1)\ ln\ f + ln(\delta_{snow,0} + 1) \quad (2)$$

$$ln(\delta_{snow} + 1) = (\alpha\text{-}1)\ ln\ c_{snow} + [ln(\delta_{snow,0} + 1) - (\alpha\text{-}1)\ ln\ c_{snow,0}] \quad (3)$$

We find in the DC04 (DC07) pit fractionation factors ε of −50±10 (−71±12) ‰, 6±3 (9±2) ‰ and 1±0.2 (2±0.6) ‰, for $\delta^{15}N$, $\delta^{18}O$ and $\Delta^{17}O$, respectively (Table 1). The 1-σ uncertainties were estimated by propagating the error in the isotopic ratios (Taylor, 1997). Although they are large due to local spatial variability (e.g. Blunier et al., 2005) and sample resolution, it is found that sign and order of magnitude of ε for the oxygen stable isotopes compare well to those determined in previous lab photolysis experiments (Table 1, Fig. 4). In DC04 the ε for $\delta^{15}N$ compares well to the literature value of −54±10‰ reported for Dome C, whereas in DC07 it falls above the upper end of the cited range of uncertainty (Table 1, Fig. 4) (Blunier et al., 2005).

ACPD
9, 12559–12596, 2009

The observed post-depositional fractionation is attributed to NO_3^- mass loss from the upper snow pack, as first suggested by Blunier et al. (2005) to explain the strong enrichment of $\delta^{15}N(NO_3^-)$ in snow at DC. Gas phase chemistry cannot be responsible for two reasons. Firstly, reactions which favor nitrate production tend to minimize the fractionation of $\delta^{15}N(NO_3^-)$ with respect to NO_x, and therefore lead to isotopic ratios close to those of atmospheric NO_x, typically ranging between −9 and 13‰ (Heaton et al., 2004). And secondly, strongly positive $\delta^{15}N(NO_3^-)$ values have never been observed in atmospheric NO_3^- in Antarctica (Wagenbach et al., 1998; Savarino et al., 2007, this study Fig. 3c).

NO_3^- mass loss from snow and therefore isotopic fractionation is thought to be governed by evaporation of HNO_3 and NO_3^- photolysis. The extent of post-depositional processing by either mechanism is in turn controlled by local accumulation rate, temperature, UV radiation and snow physical properties. Wind driven redistribution of surface snow and forced ventilation due to wind pumping may contribute as well, but are less important on a dome with average annual wind speeds of 2.8 m s^{-1}. A previous comparison has shown that at wind speeds of <3 m s^{-1} molecular diffusion rather than forced ventilation from wind pumping determines vertical movement of trace gas chemical species through the open snow pore space (Frey et al., 2005).

Surface snow samples from the DC-DDU traverse indicate to a first order that fractionation increases as annual accumulation rates decrease (data from Pettre et al., 1986). $\delta^{15}N(NO_3^-)$ are negatively correlated with annual accumulation rates (r=−0.67, p<0.01) in agreement with previous findings from Antarctic ice cores (Freyer et al., 1996), whereas $\delta^{18}O(NO_3^-)$ shows a positive correlation (r=0.68, p<0.01). NO_3^- losses were also observed at South Pole, where surface snow NO_3^- exceeds all concentration spikes preserved in the top 6 m (McCabe et al., 2007). The top snow layer, representing the most recent year of snow accumulation, shows a $\Delta^{17}O(NO_3^-)$ of 29.9‰ (median of reported max and min values of year round monthly sampling), close to 30.4‰ in atmospheric NO_3^- (median of reported max and min value), whereas at depth

ACPD
9, 12559–12596, 2009

$\Delta^{17}O(NO_3^-)$ is depleted by 4–5‰ similar to our finding at DC (McCabe et al., 2007). At Summit, Greenland, a site with a mean annual accumulation rate of 25 g $cm^{-2}yr^{-1}$ (Dibb and Fahnestock, 2004), up to 30% post-depositional loss of NO_3^- was observed (Dibb et al., 2007). However, according to one study, $\delta^{15}N(NO_3^-)$ and $\delta^{18}O(NO_3^-)$ did not change significantly over a period of 5 months, the time between initial deposition and burial to 30 cm depth by subsequent snow fall (Hastings et al., 2004).

Below we discuss in more detail how evaporation and photolysis determine the signal of stable isotopes in NO_3^- preserved in snow.

4.2 Mechanisms of isotopic fractionation in snow

It is instructive to recall what is known about location and chemical form of NO_3^- within snow grains. NO_3^- is found not only in the bulk crystal, but is adsorbed also at the top of or dissolved within the so-called quasi liquid layer (QLL) on the grain surface (e.g. Grannas et al., 2007, and references therein). In fresh snow the distribution within the snow grain depends on the specific deposition process, but is not well constrained by bulk concentrations alone (Röthlisberger et al., 2002). For example, at DC snow grains at the surface have a specific surface area of 400–450 $cm^2\,g^{-1}$ (Gallet et al., 2009) and potential HNO_3 coverage is estimated to be 1×10^{13} molec cm^{-2} (Hudson et al., 2002), which yields a NO_3^- concentration of 420–475 ng g^{-1}. Thus, concentrations observed in surface snow would be consistent with NO_3^- being located entirely on the grain surface (Fig. 1c).

Regarding the chemical form we know that in present-day Antarctica and past interglacials NO_3^- occurs predominantly as HNO_3 as opposed to the salt $Ca(NO_3)_2$ during glacials (Legrand et al., 1999). It has been suggested that HNO_3 newly adsorbed on ice ionizes in a 2-step process,

$$HNO_{3,g} + H_2O_s \rightleftharpoons HNO_3 \cdot H_2O_{ad} \rightleftharpoons NO_{3,aq}^- + H_3O_{aq}^+ \quad \text{(R6)}$$

where subscripts g, s, ad and aq denote gas, surface, adsorbed and solvated (aque-

ous) species, respectively (Pursell et al., 2002). Molecular dynamics simulations provide support for the notion that nitrate at the air-water interface remains molecular HNO_3, whereas it dissociates when embedded at various depths within the aqueous layer (e.g. Thomas et al., 2007; Wang et al., 2009). The pH and ionic strength control acid dissociation but are not well characterized in the QLL. However, in the bulk snow crystal we can assume the pH range of natural waters and an acid dissociation constant pK_a of −1.19 and find that the ionic form dominates with less than 1×10^{-4}% of total nitrate occuring as molecular HNO_3.

This is important since all forms of nitrate in Reaction (R6) will photolyze, at the surface and very likely also within the snow grain, whereas only molecular HNO_3 will evaporate from the surface (Sato et al., 2008).

4.2.1 Evaporation

Surface and wind-driven sublimation are important components of the surface mass balance in Antarctica and can remove up to 20% of annual snowfall at DC (Frezzotti et al., 2004), similar to estimates for the entire ice sheet (Dery and Yau, 2002). While insoluble chemical species will be enriched, volatile species will be removed depending on their volatility. Since surface snow at DC in summer is supersaturated in NO_3^- with respect to atmospheric HNO_3 (Röthlisberger et al., 2002) one expects physical loss, but the time scale of that loss is somewhat uncertain. Summer pit profiles of NO_3^- concentrations look always similar (Fig. 1c, Blunier et al., 2005) and concentrations in fresh snowfall exceed those at depth typically by 1–2 orders of magnitude, indicating that NO_3^- deposited in winter must be driven out of the snow within the following spring and summer. However, some observational evidence suggests that the physically driven loss of molecular HNO_3 from the snow matrix is a slow process. Dissolution of HNO_3 and therefore also release across the air-QLL interface was observed to occur within minutes (Pursell et al., 2002). But on the snow grain scale, HNO_3 diffusion measured in ice is too slow to explain rapid loss of NO_3^- over one season. For example,

ACPD
9, 12559–12596, 2009

the ice diffusion constant D_0 of HNO_3 at DC in summer is 2.5×10^{-11} $cm^2\,s^{-1}$ (Thibert and Domine, 1998) and yields for typical snow grain diameters d of 0.05–0.1 cm an average diffusion time $\tau = d^2\,(2\,D_0)^{-1}$ of 1.5–3 yr. In another study evaporation rates of dilute acids were measured above frozen solutions and found to be primarily controlled by the degree of dissociation with vapor pressure being of second order (Sato et al., 2008). This explained that evaporative losses were lowest for highly dissociated acids such as hydrochloric acid (HCl) and not detectable for HNO_3 during 96 h long experiments (Sato et al., 2008).

No experimental ε values for ice(water)-vapor phase fractionation are currently available, but in analogy to the stable isotopes in water (H_2O) one would expect net enrichment of both nitrogen and oxygen stable isotopes in the NO_3^- fraction remaining in the snow phase. Since evaporation of HNO_3 occurs in the molecular form (Sato et al., 2008), one might argue that the required recombination of NO_3^- with a proton (Reaction R6) induces depletion of the heavy oxygen isotopes in NO_3^-. This will be the case if $O_2N^{18}O$-H is energetically much favored over $O_2N^{16}O$-H. As a first-order estimate we calculate shifts in the vibrational frequencies ν for the O-H (3550 cm^{-1}) and O-NO_2 (647 cm^{-1}) stretching modes in $HNO_{3,g}$ as a result of substituting ^{16}O with ^{18}O (Table 3). Approximation of ν of the heavier isotopologue using the known relationship between vibration frequencies and reduced masses of a harmonic oscillator (e.g. Criss, 1999) yields shifts of 1 cm^{-1} and 26 cm^{-1}, for the O-H and O-NO_2 stretching modes, respectively. This indicates that isotopic replacement increases mostly the N-O bond strength, whereas the impact on the O-H bond is negligible. Dissociation/recombination of HNO_3 will therefore enrich the heavy oxygen isotopes in the ionic form.

From the above we conclude that evaporation/sublimation of HNO_3 should lead to enrichment of all the heavy isotopes in the NO_3^- fraction remaining in the snow. Estimating the order of magnitude of evaporative ε values for HNO_3 isotopologues proves more difficult. For $\delta^{18}O(H_2O)$ the ice-vapor phase fractionation factor ε was measured previously in the lab (Neumann et al., 2008) and is close to that predicted by an em-

pirical model (Majoube, 1970). Using the model and the annual temperature cycle at DC we estimate ε values ranging from −18‰ in summer to −34‰ in winter (Majoube, 1970). If $\delta^{15}N(NO_3^-)$ fractionated in a similar way upon evaporation then ε would be less negative than the bulk fractionation factors observed in the field (Table 1). Lab experiments suggest that fractionation from evaporation/sublimation is likely to be small, since no fractionation of oxygen stable isotopes was observed when cells filled with snow samples were flushed for several hours with helium gas (McCabe et al., 2005).

4.2.2 Photolysis

We evaluate photolytic fractionation by applying the theory of photo-induced isotopic fractionation effects (PHIFE) (Miller and Yung, 2000). This general framework was originally developed to explain enrichment of all the rare heavy isotopologues observed in stratospheric N_2O, a molecule whose main sink is photodissociation (Yung and Miller, 1997). The physical principal underlying PHIFE is that every isotopologue has its unique spectroscopic signature. Substitution of an atom by its heavier isotope causes an increase in reduced mass and therefore a red shift in the vibrational frequencies and a reduction in zero point energy (ΔZPE) of the molecule (Miller and Yung, 2000). This explains small blue shifts in the UV absorption spectra of the heavier isotopologues, which in turn lead to measurable differences in isotopic fractionation (Miller and Yung, 2000). PHIFE can be applied to aqueous NO_3^- due to its continuous UV absorption spectrum (Chu and Anastasio, 2003) and lack of predissociation (Miller and Yung, 2000, and references therein). We consider first the nitrogen staple isotopic enrichment and discuss oxygen further below.

$\delta^{15}N$

Since experimental spectral data on the heavy NO_3^- isotopologues in water or snow are currently not available, we estimate the UV absorption spectrum of aqueous $^{15}NO_3^-$ by shifting measured spectral absorptivities of $^{14}NO_3^-$ (Chu and Anastasio, 2003)

ACPD
9, 12559–12596, 2009

by the difference in zero point energy (ZPE) between the respective isotopologues (Fig. 5a, Yung and Miller, 1997). ZPE is calculated using ZPE=0.5 $\sum \nu_i$, where ν_i refers to the normal vibration frequencies. Vibrational frequencies for some isotopologues of aqueous NO_3^- were determined previously through measurement (Begun and Fletcher, 1960) and *ab initio* calculations (Casciotti, 2009) (Table 2). Using the data of (Begun and Fletcher, 1960) we derive a ΔZPE of $-44.85\,cm^{-1}$, equivalent to an average blueshift of 0.5 nm in the 280–360 nm region (Fig. 5a, Table 2). Convolution of spectral actinic flux $I(\lambda)$, computed with the radiation transfer model TUV4.4 (http://www.acd.ucar.edu/TUV, Madronich and Flocke, 1998) for conditions at Dome C in January 2004, quantum yield ϕ_a estimated for −30°C after Chu and Anastasio (2003) and the respective spectral UV absorptivity σ_a (Fig. 5a) yields $^{14}NO_3^-$ ($^{15}NO_3^-$) photolysis rates j (j') of $7.65\,(7.29)\times10^{-8}\,s^{-1}$ (Fig. 5b):

$$j = \int_{\lambda i}^{\lambda j} \sigma_a(\lambda)\,\phi_a(\lambda)\,I(\lambda)\,d\lambda \quad (4)$$

Calculated photolysis rates are about 80% of recent field measurements at DC (J. L. France, personal communication, 2008) and the resulting ε=(j'/j)−1 of −48‰ is close to bulk fractionation factors derived from pit profiles (Fig. 5b, Tables 1, 2). We obtain a similar ε when we use the vibrational frequencies calculated by Casciotti (2009) (Table 2). Examination of the spectral $\varepsilon(\lambda)$ shows that below 302 nm depletion should occur, however due to the nature of $I(\lambda)$ enrichment dominates (Fig. 5b). These estimates are significantly larger than the reported ε value of −11‰ derived from lab photolysis experiments (Table 1, Blunier et al., 2005; Jacobi et al., 2006). In these artificial snow made from dilute solutions of $NaNO_3$ was used, but additional tests replacing the salt solution with HNO_3 did not indicate any sensitivity of ε to the chemical form of NO_3^- (H. W. Jacobi, personal communication, 2008).

However, we suspect that ε for $\delta^{15}N(NO_3^-)$ was significantly underestimated by Blunier et al. (2005) due to the experimental set up employed. First, irradiated snow samples were kept in closed cells and therefore photolysis products NO_2 and OH not

flushed from the cell likely participated in reformation and deposition of NO_3^-, thereby reducing isotopic fractionation (Jacobi et al., 2006). NO_3^- reformation is consistent with NO_3^- concentrations never dropping below 10% of the starting levels, even after prolonged irradiation (Jacobi et al., 2006). Second, the UV spectrum of the lamp used in the experiments was significantly different from the solar one and no cut-off filters were used. It therefore extended to 230 nm and showed a secondary maximum around 302 nm (Fig. 5a, Jacobi et al., 2006). Significant contributions from shorter wavelengths to spectral actinic flux will lead to less enrichment or even depletion as the shape of the spectrally resolved $\varepsilon(\lambda)$ shows (Fig. 5b), resulting in a decrease of ε. Replacing the spectral irradiance for DC (Fig. 5a) with that of the UV lamp used by Jacobi et al. (2006) we obtain ε values of −8 to −9‰ (Table 2), very close to the lab results by Blunier et al. (2005).

With regard to the speciation of total nitrate in (Reaction R6) we consider also the case that molecular HNO_3 is subject to photolysis (e.g. Huber, 2004).

$$HNO_3 + h\nu \rightarrow NO_2 + OH \quad \text{(R7)}$$

We use observed vibration frequencies for molecular, gaseous $HNO_{3,g}$ (Guillory and Bernstein, 1975) and following the results of Casciotti (2009) assume that they do not differ much from those of $HNO_3 \cdot H_2O_{ad}$ or $HNO_3 \cdot H_2O_{aq}$. The measured σ_a spectrum of $HNO_{3,g}$ is interpolated to DC summer temperatures (Rattigan et al., 1992). We find ε values of −92 and −65‰ for vibration frequencies of matrix-isolated $HNO_{3,g}$ and observed in nitrogen (N_2), respectively (Table 3). These values are significantly more negative than those derived from DC snow pits (except DC07) and lab experiments (Tables 1, 3). Therefore nitrogen isotope fractionation is best explained by photolysis of ionic NO_3^-.

$\delta^{18}O$ and $\Delta^{17}O$

Using the same approach, we calculate also ε for the stable isotopes of oxygen in NO_3^-. Even though the only vibrational frequencies of NO_3^- isotopologues available were measured on microcrystalline KNO_3 (Chakraborty et al., 1999), use of those is warranted for two reasons. First, due to the ionic K-O bond NO_3^- in KNO_3 exhibits similar geometry and therefore similar frequencies (Chakraborty et al., 1999, Table 2). Second, differences in observed ν between solid $KNO_{3,solid}$ and aqueous $NO_{3,aq}^-$ are small, much smaller than when compared with $NO_{3,aq}^-$ from ab initio calculations (Table 2). While we obtain ε values for ^{15}N similar to the results discussed above, ε for ^{18}O range between −10 and −20‰ (Table 2). Thus, PHIFE predicts enrichment for all the heavy isotopes of NO_3^-, and therefore fails to explain the depletion of stable oxygen isotopes in NO_3^- observed in the field and lab (Tables 1, 2). It should be noted that the $\nu_{3,4}$ (NO-O stretching mode) are significantly shifted to the blue upon isotopic substitution of ^{16}O with ^{18}O (Table 2). This indicates weakening of the N-O bond and would explain depletion of the heavy oxygen isotope in the case that al the red-shifted vibrational frequencies contribute less to ZPE than assumed by the equation used above.

As opposed to ^{15}N we argue that oxygen stable isotopes will be affected by not only photolysis but also matrix effects. Previous lab photolysis experiments using isotopically labeled water suggested that oxygen isotope depletion is the result of isotopic exchange with reservoirs depleted in heavy oxygen during secondary NO_3^- formation (McCabe et al., 2005). Photolytically formed NO_2 and NO (Reactions R1–R4) are re-oxidized in aqueous phase reactions with the OH radical, produced mostly from H_2O_2 photolysis (Anastasio et al., 2007), and water, e.g. in the QLL, to NO_3^- and NO_2^-, respectively. $\delta^{18}O(H_2O)$ of Antarctic snow is <-40‰ (Masson-Delmotte et al., 2008) and $\delta^{18}O$ of the OH radical likely similar due to rapid exchange with H_2O in the aqueous phase (Meijer and Li, 1998). Isotopic exchange with OH and H_2O also explains the decrease of $\Delta^{17}O(NO_3^-)$ since both reservoirs have $\Delta^{17}O$ close to zero (McCabe et al.,

ACPD
9, 12559–12596, 2009

2005, and references therein).

4.3 NO_3^- recycling above snow in Antarctica

We have shown that photolysis can explain ε values derived from field observations and lab experiments, where evaporation/sublimation was minimal or not occuring at all. Since fractionation is associated with mass loss, this is strong evidence for UV-photolysis being the main process that drives NO_3^- out of the snow pack at DC and very likely across the low accumulation regions of East Antarctica. This has implications for the interpretation of the annual variability of isotopic ratios in atmospheric NO_3^- (Fig. 3) and atmosphere-snow cycling of NO_3^- above the EAIS. In Antarctica, primary NO_3^- sources are thought to be sedimentation of polar stratospheric clouds (PSCs) in late winter and a background tropospheric source from lightning, biomass burning and the ocean (Wagenbach et al., 1998; Savarino et al., 2007). On the one hand, the spring maximum of atmospheric NO_3^- concentrations observed on the coast and now also inland (Fig. 3b) was recently attributed to a stratospheric source based on the $\Delta^{17}O(NO_3^-)$ signature (Fig. 3e, Savarino et al., 2007). On the other hand, it has been suggested that the coastal summer maximum of NO_3^- concentrations (Fig. 3b) has its origin in reoxidized snow emissions of reactive nitrogen advected from the interior of Antarctica (Savarino et al., 2007). This was based on the argument that surface snow enrichment implies emissions depleted in $^{15}N(NO_3^-)$ along with the observation of strongly negative δ^{15} in atmospheric NO_3^- in summer. Strongly negative δ^{15} in atmospheric NO_3^- from snow emissions have been observed also in the Weddel sea sector and the Arctic (Morin et al., 2008, 2009).

To understand better the significant difference in the annual cycles of atmospheric $\delta^{15}N(NO_3^-)$ between DC and the coast (Fig. 3c) we apply again the Rayleigh model to calculate $\delta^{15}N(NO_3^-)$ in the snow and emission fraction as a function of NO_3^- mass loss (Fig. 6, e.g. Criss, 1999). We use an ε of −54‰ and as the initial $\delta^{15}N(NO_3^-)$ in snow a value of 19‰ expected in late winter snow fall from a previous estimate for

ACPD
9, 12559–12596, 2009

stratospheric NO_3^- (Savarino et al., 2007). We consider two emission scenarios, one, immediate removal after release i.e. via horizontal transport (case 1, Fig. 6) and two, accumulation of emissions above the local snow surface, equivalent to the integration of all emissions from case 1 (case 2, Fig. 6). Continuous NO_3^- loss leads to strong isotopic enrichment in the snow fraction consistent with the isotopic ratios found in the upper snow pack (Figs. 6, 1c). However, the profiles of NO_3^- concentration and $\delta^{15}N(NO_3^-)$ indicate that NO_3^- loss is not uniform with depth (Fig. 1c). We therefore suggest the existence of two regions, a skin layer with isotope ratios close to atmospheric equilibrium and high NO_3^- concentrations and the snow pack underneath strongly depleted in NO_3^- and therefore enriched in $\delta^{15}N$.

The assumption of isotopic equilibrium at the surface is supported two-fold. First, photolysis dominating NO_3^- loss from the snow pack implies that reactive nitrogen released to the open snow pore space and atmosphere occurs mainly as NO_x or HONO, as opposed to gaseous HNO_3 in the case of evaporation. Physical interaction with the snow crystal surface will be much smaller for the former than for the latter. Gas phase molecular diffusion with characteristic times on the order of minutes suffices to quickly transfer the photolysis products upward through the firn-air column into the atmosphere above the snow, where eventually all reduced species are oxidized again to NO_3^- and redeposited to the surface. The photochemical lifetime of NO_x in summer above the plateau is short with ~15 h (Davis et al., 2008), consistent with rapid recycling at the surface and thereby establishing isotopic equilibrium. Second, $\delta^{15}N(NO_3^-)$ values in the skin layer at DC in summer are close to those found in atmospheric NO_3^- (Frey et al., 2009). It should be noted that this is apparently not the case for the top samples in the DC04 and DC07 pits, as they are enriched compared to the atmospheric signal (Figs. 1c, 3c). However, this is due to the chosen sample depth resolution, since collection including snow from below the skin layer (e.g. the top 0.5 cm) will necessarily result in increased isotopic ratios.

Calculated isotope ratios of emissions in case 2 match best the observed recovery from strongly negative $\delta^{15}N(NO_3^-)$ to back ground levels in atmospheric NO_3^- at DC

ACPD
9, 12559–12596, 2009

(Figs. 3c, 6). The exact match with December observations is fortuitous and depends on the initial isotopic ratio chosen for winter snow fall. However, extremely positive $\delta^{15}N(NO_3^-)$ as predicted by case 1 scenario have never been observed. Therefore, we conclude that no significant mass export i.e. by horizontal transport is likely to occur neither at DC nor above the entire EAIS plateau region, where environmental parameters are similar (Figs. 3, 6). One implication of minimal NO_3^- export off the EAIS plateau is that transport strength, a parameter considered to further complicate the interpretation of NO_3^- ice core records (Wolff et al., 2008), is likely not to play an important role for ice cores recovered from that region.

As discussed above, NO_3^- loss from the snow pack is much smaller in regions with higher annual accumulation rates (Dibb et al., 2007), including those close to the coast. According to the model $\delta^{15}N(NO_3^-)$ of emissions remain therefore strongly depleted, consistent with observations during spring and summer at all coastal sites (Figs. 3c, 6). Surface snow collected towards the coast shows also negative $\delta^{15}N(NO_3^-)$, as expected from isotopic equilibrium between atmosphere and snow (Fig. 2a). However, it is not possible to distinguish between case 1 and 2, thus leaving open the possibility of NO_3^- export and emissions from a region reaching as far inland as the 2700 m contour line could contribute to the DDU summer maximum (Figs. 2a, 6), consistent with the hypothesis stated by Savarino et al. (2007).

5 Conclusions

Findings from the first combined atmosphere-snow study of the comprehensive NO_3^- stable isotopic composition in Antarctica have important implications for our ability to interpret the isotopic signal preserved in snow and ice and our understanding of reactive nitrogen cycling in the low accumulation regions of EAIS.

First, profiles of nitrogen (oxygen) stable isotopes of NO_3^- in surface-near snow at DC show strong enrichment (depletion) compared to the isotopic signal registered in atmospheric NO_3^- and thus reflect post-depositional fractionation associated with NO_3^-

ACPD
9, 12559–12596, 2009

mass loss rather than atmospheric trends. In contrast, post-depositional effects on $\Delta^{17}O(NO_3^-)$ signal in snow are relatively small. Although the stratospheric source signature and information on seasonal changes in NO_3^- formation pathways (e.g. Morin et al., 2008) are not preserved, atmospheric trends of lower frequency (e.g. the 2.7 yr cycle) survive post-depositional processing. It therefore seems possible to reconstruct past shifts in tropospheric oxidation pathways from the $\Delta^{17}O(NO_3^-)$ record preserved in ice cores. On the other hand, use of $\delta^{18}O(NO_3^-)$ as a tracer for atmospheric NO_3^- oxidation pathways (e.g. Hastings et al., 2005; Jarvis et al., 2008) is discouraged, due to its sensitivity to post–depositional fractionation. Second, we provide strong evidence that UV–photolysis is the dominant process responsible for the NO_3^- loss from snow observed at DC. $\delta^{15}N(NO_3^-)$ fractionation associated with the mass loss can be explained quantitatively by NO_3^- photolysis alone. Lab values reported previously are too low as the UV lamp used is not representative for the solar surface spectrum at DC (Blunier et al., 2005). We attribute the observed depletion of oxygen stable isotopes in NO_3^- to matrix effects, which require also NO_3^- photolysis followed by isotopic exchange between photolysis products and H_2O and OH. Isotopic effects from evaporation will likely be small, however require still experimental quantification. Third, as a conceptual model for NO_3^- recycling in the atmosphere-system for DC and the entire EAIS where annual accumulation is low we suggest the following: stratospheric NO_3^- is deposited to the surface in late winter in a shallow surface snow layer of approximately uniform concentration and $\delta^{15}N(NO_3^-)$. The increase in surface UV–radiation in spring then initiates a photolysis driven redistribution process of NO_3^-, which continues throughout the sunlit season resulting in almost complete depletion of the bulk reservoir. This leads then in summer to a strongly asymmetric distribution of total NO_3^- within the atmosphere-snow column as noted previously (Wolff et al., 2002), with the bulk residing in a skin layer and only a small fraction in the atmospheric column above it.

On going year-round atmosphere-snow studies and summer intensive campaigns at DC will contribute to the development of a quantitative model and specifically address

ACPD
9, 12559–12596, 2009

time-scales and mass fluxes involved in the NO_3^- redistribution process. Further lab studies are needed also to quantify the evaporative fractionation factor for nitrogen and oxygen stable isotopes in NO_3^-.

Acknowledgements. This work has been made possible thanks to the partial support from the European Science Foundation (ESF) under the EUROCORES Programme EuroCLIMATE, through contract No. ERAS-CT-2003-980409 of the European Commission, DG Research, FP6. Partial funding has also been provided by the National Research Agency of France through project ANR-07-VULN-013 VANISH. We thank D. M. Sigman for making available the denitrifier method, E. Vince and P. Donnadieu for helping with the lab analysis, as well as IPEV for providing logistics, Dome C staff for sample collection and PNRA for DC meteorological data. Discussions with K. Frey were helpful in improving this manuscript.

The publication of this article is financed by CNRS-INSU.

References

Anastasio, C., Galbavy, E. S., Hutterli, M. A., Burkhart, J. F., and Friel, D. K.: Photoformation of hydroxyl radical on snow grains at Summit, Greenland, Atmos. Environ., 41, 5110–5121, 2007. 12562, 12576

Baertschi, P.: Absolute ^{18}O content of the Standard Mean Ocean Water, Earth Planet. Sc. Lett., 31(3), 341–344, 1976. 12564

Begun, G. M. and Fletcher, W. H.: Partion function ratios for molecules containing nitrogen isotopes, J. Chem. Phys., 33, 1083–1085, 1960. 12574, 12589

Blunier, T., Floch, G. L., Jacobi, H. W., and Quansah, E.: Isotopic view on nitrate loss in Antarctic surface snow, Geophys. Res. Lett., 32, L13501, doi:10.1029/2005GL023011, 2005.

12560, 12561, 12562, 12566, 12567, 12568, 12569, 12571, 12574, 12575, 12580, 12588, 12596

Böhlke, J. K., Mroczkowski, S. J., and Coplen, T. B.: Oxygen isotopes in nitrate: new reference materials for ^{18}O:^{17}O:^{16}O measurements and observations on nitrate-water equilibration, Rapid Commun. Mass Sp., 17, 1835–1846, 2003. 12564

Boxe, C. S. and Saiz-Lopez, A.: Multiphase modeling of nitrate photochemistry in the quasi-liquid layer (QLL): implications for NO_x release from the Arctic and coastal Antarctic snowpack, Atmos. Chem. Phys., 8, 4855–4864, 2008, http://www.atmos-chem-phys.net/8/4855/2008/. 12562

Casciotti, K. L.: Inverse kinetic isotope fractionation during bacterial nitrite oxidation, Geochim. Cosmochim. Ac., 73, 2061–2076, doi:10.1016/j.gca.2008.12.022, 2009. 12574, 12575, 12589

Casciotti, K. L., Sigman, D. M., Hastings, M. G., Bohlke, J. K., and Hilkert, A.: Measurement of the oxygen isotopic composition of nitrate in seawater and freshwater using the denitrifier method, Anal. Chem., 74, 4905–4912, 2002. 12564

Chakraborty, T., Bajpai, P. K., and Verma, A. L.: Room temperature spectroscopic investigations of $K^{14}NO_3$, $K^{15}NO_3$, $KNO_{3-x}{}^{18}O_x$ and a 1 : 1 mixture of $K^{14}NO_3$ and $K^{15}NO_3$: Intermolecular coupling revealed in the vibrational spectra, J. Raman Spectrosc., 30, 189–194, 1999. 12576, 12589

Chu, L. and Anastasio, C.: Quantum yields of hydroxyl radical and nitrogen dioxide from the photolysis of nitrate on ice, J. Phys. Chem. A, 107, 9594–9602, 2003. 12562, 12573, 12574, 12595

Criss, R. E.: Principles of stable isotope distribution, Oxford University Press, 1999. 12572, 12577

Davis, D. D., Seelig, J., Huey, G., Crawford, J., Chen, G., Wang, Y. H., Buhr, M., Helmig, D., Neff, W., Blake, D., Arimoto, R., and Eisele, F.: A reassessment of Antarctic plateau reactive nitrogen based on ANTCI 2003 airborne and ground based measurements, Atmos. Environ., 42, 2831–2848, doi:10.1016/j.atmosenv.2007.07.039, 2008. 12578

Dery, S. J. and Yau, M. K.: Large-scale mass balance effects of blowing snow and surface sublimation, J. Geophys. Res., 107, 4679, doi:10.1029/2001JD001251, 2002. 12571

Dibb, J. E. and Fahnestock, M.: Snow accumulation, surface height change, and firn densification at Summit, Greenland: Insights from 2 years of in situ observation, J. Geophys. Res., 109, D24113, doi:10.1029/2003JD004300, 2004. 12570

Dibb, J. E., Whitlow, S. I., and Arsenault, M.: Seasonal variations in the soluble ion content of snow at Summit. Greenland: Constraints from three years of daily surface snow samples, Atmos. Environ., 41, 5007–5019, doi:10.1016/j.atmosenv.2006.12.010, 2007. 12570, 12579, 12596

Frey, M. M., Stewart, R. W., McConnell, J. R., and Bales, R. C.: Atmospheric hydroperoxides in West Antarctica: links to stratospheric ozone and atmospheric oxidation capacity, J. Geophys. Res., 110, D23301, doi:10.1029/2005JD006110, 2005. 12569

Frey, M. M., Bales, R. C., and McConnell, J. R.: Climate sensitivity of the century-scale hydrogen peroxide (H_2O_2) record preserved in 23 ice cores from West Antarctica, J. Geophys. Res., 111, D21301, doi:10.1029/2005JD006816, 2006. 12564, 12567

Frey, M. M., Savarino, J., Erbland, J., and Morin S., in preparation, 2009. 12565, 12566, 12578

Freyer, H. D., Kobel, K., Delmas, R. J., Kley, D., and Legrand, M. R.: First results of $^{15}N/^{14}N$ ratios in nitrate from alpine and polar ice cores, Tellus B, 48, 93–105, 1996. 12567, 12569

Frezzotti, M., Pourchet, M., Flora, O., Gandolfi, S., Gay, M., Urbini, S., Vincent, C., Becagli, S., Gragnani, R., Proposito, M., Severi, M., Traversi, R., Udisti, R., and Fily, M.: New estimations of precipitation and surface sublimation in East Antarctica from snow accumulation measurements, Clim. Dynam., 23, 803–813, doi:10.1007/s00382-004-0462-5, 2004. 12571

Gallet, J. C., Arnaud, L., and Domine, F.: Specific surface area of snow at Dome C, Antarctica. Rates of change for timescales from 1 day to 60 years, Geophys. Res. Abstr., EGU2009-4270, 2009. 12570

Grannas, A. M., Jones, A. E., Dibb, J., Ammann, M., Anastasio, C., Beine, H. J., Bergin, M., Bottenheim, J., Boxe, C. S., Carver, G., Chen, G., Crawford, J. H., Dominé, F., Frey, M. M., Guzmán, M. I., Heard, D. E., Helmig, D., Hoffmann, M. R., Honrath, R. E., Huey, L. G., Hutterli, M., Jacobi, H. W., Klán, P., Lefer, B., McConnell, J., Plane, J., Sander, R., Savarino, J., Shepson, P. B., Simpson, W. R., Sodeau, J. R., von Glasow, R., Weller, R., Wolff, E. W., and Zhu, T.: An overview of snow photochemistry: evidence, mechanisms and impacts, Atmos. Chem. Phys., 7, 4329–4373, 2007, http://www.atmos-chem-phys.net/7/4329/2007/. 12561, 12562, 12570

Guillory, W. A. and Bernstein, M. L.: Infrared-Spectrum of matrix-isolated nitric acid, J. Chem. Phys., 62, 1058–1060, 1975. 12575, 12590

Hastings, M. G., Steig, E. J., and Sigman, D. M.: Seasonal variations in N and O isotopes of nitrate in snow at Summit, Greenland: Implications for the study of nitrate in snow and ice cores, J. Geophys. Res., 109, D20306, doi:10.1029/2004JD004991, 2004. 12561, 12567,

12570
Hastings, M. G., Sigman, D. M., and Steig, E. J.: Glacial/interglacial changes in the isotopes of nitrate from the Greenland Ice Sheet Project 2 (GISP2) ice core, Global Biogeochem. Cy., 19, GB4024, doi:10.1029/2005GB002502, 2005. 12580
Heaton, T. H. E., Wynn, P., and Tye, A. M.: Low $^{15}N/^{14}N$ ratios for nitrate in snow in the High Arctic (79°N), Atmos. Environ., 38, 5611–5621, doi:10.1016/j.atmosenv.2004.06.028, 2004. 12567, 12569
Huber, J. R.: Photochemistry of molecules relevant to the atmosphere: Photodissociation of nitric acid in the gas phase, ChemPhysChem, 5, 1663–1669, doi:10.1002/cphc.200400071, 2004. 12575
Hudson, P. K., Shilling, J. E., Tolbert, M. A., and Toon, O. B.: Uptake of nitric acid on ice at tropospheric temperatures: Implications for cirrus clouds, J. Phys. Chem. A, 106, 9874–9882, doi:10.1021/jp020508j, 2002. 12570
Jacobi, H. W., Annor, T., and Quansah, E.: Investigation of the photochemical decomposition of nitrate, hydrogen peroxide, and formaldehyde in artificial snow, J. Photoch. Photobio. A, 179, 330–338, 2006. 12574, 12575, 12588, 12589, 12590, 12595
Jarvis, J. C., Steig, E. J., Hastings, M. G., and Kunasek, S. A.: Influence of local photochemistry on isotopes of nitrate in Greenland snow, Geophys. Res. Lett., 35, L21804, doi:10.1029/2008GL035551, 2008. 12561, 12580
Kaiser, J., Hastings, M. G., Houlton, B. Z., Röckmann, T., and Sigman, D. M.: Triple Oxygen Isotope Analysis of Nitrate Using the Denitrifier Method and Thermal Decomposition of N_2O, Anal. Chem., 79, 599–607, doi:10.1021/ac061022s, 2007. 12564
Kunasek, S. A., Alexander, B., Steig, E. J., Hastings, M. G., Gleason, D. J., and Jarvis, J. C.: Measurements and modeling of $\Delta^{17}O$ of nitrate in snowpits from Summit, Greenland, J. Geophys. Res., 113, D24302, doi:10.1029/2008JD010103, 2008. 12561, 12567
Legrand, M. R. and Delmas, R. J.: Soluble impurities in four Antarctic ice cores over the last 30 000 years, Ann. Glaciol., 10, 116–120, 1988. 12567
Legrand, M. R., Wolff, E. W., and Wagenbach, D.: Antarctic aerosol and snow fall chemistry: Implications for deep Antarctic ice core chemistry, Ann. Glaciol., 29, 66–72, 1999. 12561, 12570
Li, W. J., Ni, B. L., Jin, D. Q., and Zhang, Q. G.: Measurement of the absolute abundance of oxygen-17 in V-SMOW, Kexue Tongbao – Chinese Sci. Bull., 33, 1610–1613, 1988. 12564
Madronich, S. and Flocke, S.: The role of solar radiation in atmospheric chemistry, in: Hand-

book of Environmental Chemistry, edited by: Boule, P., Springer Verlag, Heidelberg, 1–26, 1998. 12574
Majoube, M.: Fractionation factor of ^{18}O between water vapour and ice, Nature, 226, 1242–1242, doi:10.1038/2261242a0, 1970. 12573
Mariotti, A.: Atmospheric nitrogen is a reliable standard for natural ^{15}N abundance measurements, Nature, 303, 685–687, 1983. 12564
Masson-Delmotte, V., Hou, S., Ekaykin, A., Jouzel, J., Aristarain, A., Bernardo, R. T., Bromwich, D., Cattani, O., Delmotte, M., Falourd, S., Frezzotti, M., Gallee, H., Genoni, L., Isaksson, E., Landais, A., Helsen, M. M., Hoffmann, G., Lopez, J., Morgan, V., Motoyama, H., Noone, D., Oerter, H., Petit, J. R., Royer, A., Uemura, R., Schmidt, G. A., Schlosser, E., Simoes, J. C., Steig, E. J., Stenni, B., Stievenard, M., van den Broeke, M. R., de Wal, R. S. W. V., de Berg, W. J. V., Vimeux, F., and White, J. W. C.: A review of Antarctic surface snow isotopic composition: Observations, atmospheric circulation, and isotopic modeling, J. Climate, 21, 3359–3387, doi:10.1175/2007JCLI2139.1, 2008. 12576
McCabe, J. R., Boxe, C. S., Colussi, A. J., Hoffmann, M. R., and Thiemens, M. H.: Oxygen isotopic fractionation in the photochemistry of nitrate in water and ice, J. Geophys. Res., 110, D15310, doi:10.1029/2004JD005484, 2005. 12573, 12576, 12588, 12589
McCabe, J. R., Thiemens, M. H., and Savarino, J.: A record of ozone variability in South Pole Antarctic snow: Role of nitrate oxygen isotopes, J. Geophys. Res., 112, D12303, doi:10.1029/2006JD007822, 2007. 12561, 12566, 12567, 12568, 12569, 12570
Meijer, H. A. J. and Li, W. J.: The use of electrolysis for accurate delta O-17 and delta O-18 isotope measurements in water, Isot. Environ. Healt. S., 34, 349–369, 1998. 12576
Miller, C. E. and Yung, Y. L.: Photo-induced isotopic fractionation, J. Geophys. Res., 105(D23), 29039–29051, 2000. 12573
Morin, S., Savarino, J., Frey, M. M., Yan, N., Bekki, S., Bottenheim, J. W., and Martins, J. M. F.: Tracing the Origin and Fate of NO_x in the Arctic Atmosphere Using Stable Isotopes in Nitrate, Science, 322, 730–732, doi:10.1126/science.1161910, 2008. 12561, 12564, 12577, 12580
Morin, S., Savarino, J., Frey, M. M., Domine, F., Jacobi, H.-W., Kaleschke, L., and Martins, J. M. F.: Comprehensive isotopic composition of atmospheric nitrate in the Atlantic Ocean boundary layer from 65 S to 79 N, J. Geophys. Res., 114, D05303, doi:10.1029/2008JD010696, 2009. 12561, 12564, 12577
Mulvaney, R. and Wolff, E. W.: Evidence for Winter Spring Denitrification of the Stratosphere in the Nitrate Record of Antarctic Firn Cores, J. Geophys. Res., 98(D3), 5213–5220, 1993.

12561
Mulvaney, R., Wagenbach, D., and Wolff, E. W.: Postdepositional change in snowpack nitrate from observation of year-round near-surface snow in coastal Antarctica, J. Geophys. Res., 103, 11021–11031, 1998. 12561
Neumann, T. A., Albert, M. R., Lomonaco, R., Engel, C., Courville, Z., and Perron, F.: Experimental determination of snow sublimation rate and stable-isotopic exchange, Ann. Glaciol., 49, 1–6, 2008. 12572
Pettre, P., Pinglot, J. F., Pourchet, M., and Reynaud, L.: Accumulation distribution in Terre Adelie, Antarctica – Effect of meteorological parameters, J. Glaciol., 32, 486–500, 1986. 12563, 12569
Pursell, C. J., Everest, M. A., Falgout, M. E., and Sanchez, D. D.: Ionization of nitric acid on ice, J. Phys. Chem. A, 106, 7764–7768, doi:10.1021/jp025697k, 2002. 12571
Rattigan, O., Lutman, E., Jones, R. L., Cox, R. A., Clemitshaw, K., and Williams, J.: Temperature-dependent absorption cross-sections of gaseous nitric acid and methyl nitrate, J. Photoch. Photobio. A, 66, 313–326, doi:10.1016/1010-6030(92)80003-E, 1992. 12575
Röthlisberger, R., Hutterli, M. A., Sommer, S., Wolff, E. W., and Mulvaney, R.: Factors controlling nitrate in ice cores: Evidence from the Dome C deep ice core, J. Geophys. Res., 105, 20565–20572, 2000. 12566, 12567, 12591
Röthlisberger, R., Hutterli, M. A., Wolff, E. W., Mulvaney, R., Fischer, H., Bigler, M., Goto-Azuma, K., Hansson, M. E., Ruth, U., Siggaard-Andersen, M. L., and Steffensen, J. P.: Nitrate in Greenland and Antarctic ice cores: a detailed description of post-depositional processes, Ann. Glaciol., 35, 209–216, 2002. 12561, 12570, 12571
Sato, K., Takenaka, N., Bandow, H., and Maeda, Y.: Evaporation loss of dissolved volatile substances from ice surfaces, J. Phys. Chem. A, 112, 7600–7607, 2008. 12571, 12572
Savarino, J., Kaiser, J., Morin, S., Sigman, D. M., and Thiemens, M. H.: Nitrogen and oxygen isotopic constraints on the origin of atmospheric nitrate in coastal Antarctica, Atmos. Chem. Phys., 7, 1925–1945, 2007, http://www.atmos-chem-phys.net/7/1925/2007/. 12561, 12564, 12566, 12569, 12577, 12578, 12579, 12593
Sigman, D. M., Casciotti, K. L., Andreani, M., Barford, C., Galanter, M., and Bohlke, J. K.: A bacterial method for the nitrogen isotopic analysis of nitrate in seawater and freshwater, Anal. Chem., 73, 4145–4153, 2001. 12564
Silva, S. R., Kendall, C., Wilkison, D. H., Ziegler, A. C., Chang, C. C. Y., and Avanzino, R. J.: A new method for collection of nitrate from fresh water and the analysis of nitrogen and oxygen

isotope ratios, J. Hydrol., 228, 22–36, 2000. 12563
Taylor, J. R.: An Introduction to Error Analysis: The study of uncertainties in physical measurements, University Science Books, 2nd edn., 1997. 12565, 12568, 12588
Thibert, E. and Domine, F.: Thermodynamics and kinetics of the solid solution of HNO_3 in ice, J. Phys. Chem. B, 102, 4432–4439, 1998. 12572
Thomas, J. L., Roeselova, M., Dang, L. X., and Tobias, D. J.: Molecular dynamics simulations of the solution-air interface of aqueous sodium nitrate, J. Phys. Chem. A, 111, 3091–3098, doi:10.1021/jpl0683972, 2007. 12571
Wagenbach, D., Legrand, M., Fischer, H., Pichlmayer, F., and Wolff, E. W.: Atmospheric near-surface nitrate at coastal Antarctic sites, J. Geophys. Res., 103, 11007–11020, 1998. 12566, 12569, 12577, 12593
Wang, S. Z., Bianco, R., and Hynes, J. T.: Depth-dependent dissociation of nitric acid at an aqueous surface: Car-Parrinello molecular dynamics, J. Phys. Chem. A, 113, 1295–1307, doi:10.1021/jp808533y, 2009. 12571
Wolff, E. W. and Delmas, R. J.: Nitrate in Polar Ice, in: Ice Core Studies of Global Biogeochemical Cycles, edited by: Delmas, R. J., Springer Verlag, NATO ASI Series I, 30, 195–224, 1995. 12561
Wolff, E. W., Jones, A. E., Martin, T. J., and Grenfell, T. C.: Modelling photochemical NO_x production and nitrate loss in the upper snowpack of Antarctica, Geophys. Res. Lett., 29(20), 1944, doi:10.1029/2002GL015823, 2002. 12562, 12580
Wolff, E. W., Jones, A. E., Bauguitte, S. J.-B., and Salmon, R. A.: The interpretation of spikes and trends in concentration of nitrate in polar ice cores, based on evidence from snow and atmospheric measurements, Atmos. Chem. Phys., 8, 5627–5634, 2008, http://www.atmos-chem-phys.net/8/5627/2008/. 12561, 12579
Yung, Y. L. and Miller, C. E.: Isotopic fractionation of stratospheric nitrous oxide, Science, 278, 1778–1780, 1997. 12573, 12574

Table 1. NO_3^- stable isotope fractionation factors ε[a] observed in surface snow at Dome C and recent lab photolysis experiments.

Temp., °C	ε, $\Delta^{17}O(NO_3^-)$	$\delta^{18}O(NO_3^-)$	$\delta^{15}N(NO_3^-)$	Reference
Dome C				
−54	0.9±0.2	6.4±2.5	−49.8±10.4	DC04 pit (this study)
−54	2.0±0.6	8.8±2.1	−71.0±11.7	DC07 pit (this study)
−54	–	–	−53.9±9.7	Blunier et al. (2005)
Laboratory				
−5[b]	5.3±5.4	6.9±1.3	–	McCabe et al. (2005)
−30[b]	1.2±0.3	7.0±1.6	–	McCabe et al. (2005)
−5[c]	−0.2±0.2	4.8±4.9	–	McCabe et al. (2005)
−30[c]	0.3±0.3	2.2±0.7	–	McCabe et al. (2005)
−20[d]	–	–	−11.4±1.4	Blunier et al. (2005)

[a] respective 1-σ uncertainties of ε values are based on propagation of the error in isotopic ratios (this study, after Taylor, 1997), Monte Carlo analysis (results from Blunier et al., 2005) and standard deviation of all experiments (results from McCabe et al., 2005) .

[b] artificial snow of 620 µg g^{-1} USGS-35 ($NaNO_3$), >70% NO_3^- loss after 12–48 h irradiation.

[c] artificial snow of 620 µg g^{-1} KNO_3, >70% NO_3^- loss after 12–48 h irradiation.

[d] artificial snow of 560 ng g^{-1} $NaNO_3$, max. 90% NO_3^- loss after 5 h irradiation (Jacobi et al., 2006).

ACPD
9, 12559–12596, 2009

Table 2. Normal vibrational frequencies of NO_3^- isotopologues used to calculate photolytic fractionation factors ε.

	$NO_{3,aq}^{-}$ [a] $^{14}NO_3^-$	$^{15}NO_3^-$	$NO_{3,aq}^{-}$ [b] $^{14}NO_3^-$	$^{15}NO_3^-$	$KNO_{3,solid}$ [c] $K^{14}NO_3$	$K^{15}NO_3$	$KN^{16}O_2^{18}O$
ν_i, cm^{-1}							
ν_1	1089.31	1089.31	1049.2	1049.2	1049.0	1049.0	1030
ν_2	829.003	807.405	830.9	809	834.3	811.133	822.6
ν_3	1438.45	1404.62	1375.6	1343.7	1357.5	1323.0	1370
ν_4	1438.68	1404.82	1375.6	1343.7	1357.5	1323.0	1370
ν_5	708.514	706.678	716.8	714.8	715.85	713.4	699.6
ν_6	708.8	706.953	716.8	714.8	715.85	713.4	699.6
ZPE, cm^{-1}	3106.379	3059.893	3032.45	2987.6	3015.0	2966.417	2995.9
ΔZPE, cm^{-1}	−46.486		−44.85		−48.583		−19.1
ε at DC[d],	−49.3		−47.6		−51.5		−20.3
ε Lab,	−8.4[e]		−8.1[e]		−8.8[e]		−10.3[f]

[a] aqueous phase ab initio calculations (Casciotti, 2009).
[b] aqueous phase observations (Begun and Fletcher, 1960).
[c] average IR wavenumbers observed on microcrystalline KNO_3 isotopologues (Chakraborty et al., 1999).
[d] with $I(\lambda)$ modeled for conditions at DC in January 2004 (see text).
[e] with $I(\lambda)$ of the UV lamp used in lab photolysis experiments by Jacobi et al. (2006) (see text).
[f] with $I(\lambda)$ of the UV lamp used by McCabe et al. (2005).

ACPD
9, 12559–12596, 2009

Table 3. Normal vibrational frequencies of gaseous HNO_3 isotopologues used to calculate photolytic fractionation factors ε (Guillory and Bernstein, 1975).

	$HNO_{3,g}$[a] $H^{14}NO_3$	$H^{15}NO_3$	$HNO_{3,g}$[b] $H^{14}NO_3$	$H^{15}NO_3$
ν_i, cm^{-1}				
ν_1	3490	3488	3550	3550
ν_2	1697	1659	1708	1672
ν_3	1343	1339	1330	1327
ν_4	1311	1294	1324	1321
ν_5	902	892	879	871
ν_6	767	746	762	744
ν_7	660	658	647	647
ν_8	597	594	579	578
ν_9	479	479	456	456
ZPE, cm^{-1}	5623	5574	5617.5	5583
ΔZPE, cm^{-1}	−48.5		−34.5	
ε at DC[c],	−92.4		−64.7	
ε Lab[d],	−39.0		−27.7	

[a] matrix-isolated gas phase observation.
[b] gas phase observation in N_2.
[c] with $I(\lambda)$ modeled for conditions at DC in January 2004 (see text).
[d] with $I(\lambda)$ of the UV lamp used in lab photolysis experiments by Jacobi et al. (2006) (see text).

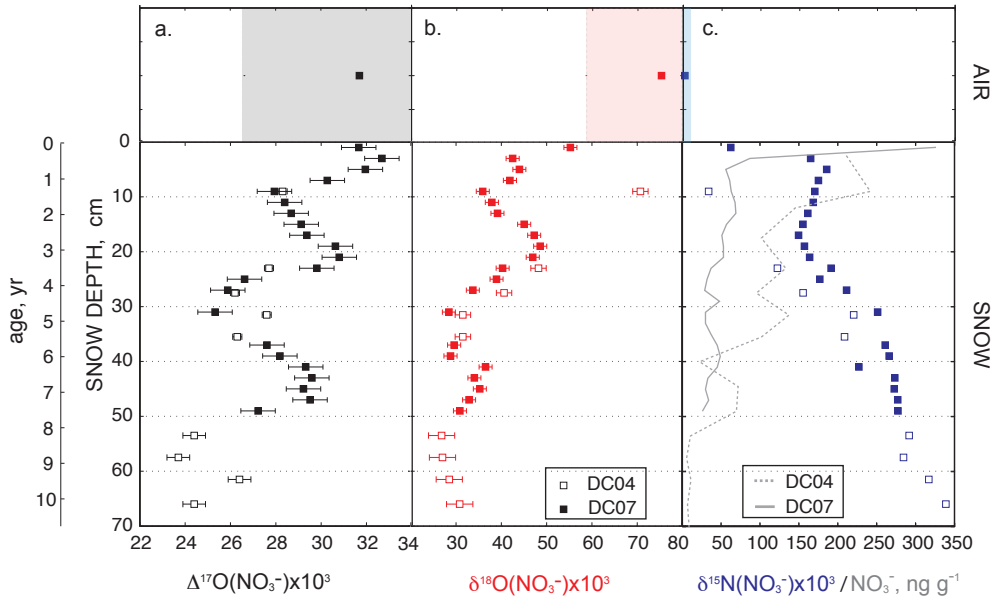

Fig. 1. $\Delta^{17}O$, $\delta^{18}O$ and $\delta^{15}N$ of NO_3^- at Dome Concordia, East Antarctica. Top panels **(a–c)**: mass-weighted averages $\pm 1\sigma$ (symbols and shaded area) in the annual cycle of atmospheric NO_3^- in 2007. Bottom panels a–c: NO_3^- in snow from pits collected in 2004 and 2007 with errorbars indicating the analytical error. NO_3^- snow concentrations are shown in bottom panel of c (dashed and solid lines). The depth-age scale is based on measured densities and a mean annual accumulation rate of 2.7 g cm^{-2} yr^{-1} (Röthlisberger et al., 2000).

ACPD
9, 12559–12596, 2009

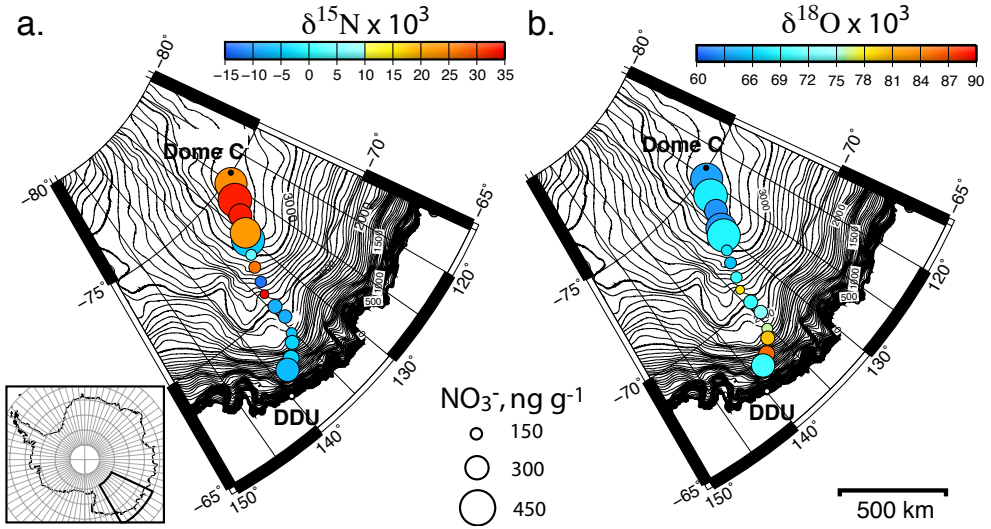

Fig. 2. Spatial distribution of $\delta^{15}N(NO_3^-)$, $\delta^{18}O(NO_3^-)$ and NO_3^- concentrations in surface snow between Dome Concordia and Dumont d'Urville.

ACPD
9, 12559–12596, 2009

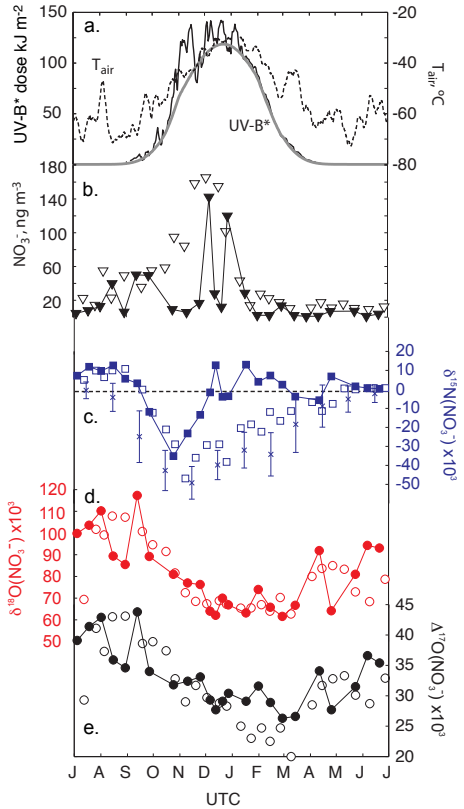

Fig. 3. Atmospheric NO_3^- at DC in 2007 and coastal records at DDU (Savarino et al., 2007) and Neumayer (NM) (Wagenbach et al., 1998): **(a)** DC air temperature and modeled daily UV-B (280–320 nm) for observed and a constant (290 DU) O_3 column density (black and grey lines) **(b)** NO_3^- concentrations, **(c)** $\delta^{15}N(NO_3^-)$, **(d)** $\delta^{18}O(NO_3^-)$ and **(e)** $\Delta^{17}O(NO_3^-)$ at DC and DDU in 2001 (closed and open symbols, respectively). Cross symbols in (c) are mean $\delta^{15}N(NO_3^-)$ at NM from 1986–1992 and errorbars the 1σ interannual variability.

ACPD
9, 12559–12596, 2009

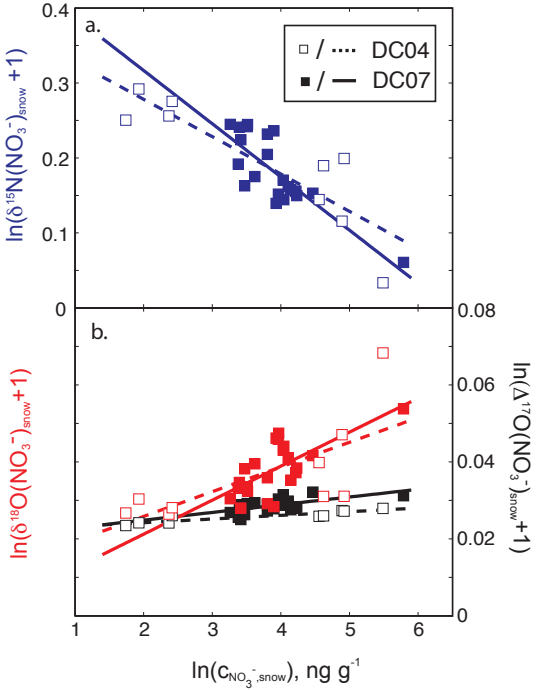

Fig. 4. Rayleigh model fit to observations of $\Delta^{17}O$, $\delta^{18}O$ and $\delta^{15}N$ of NO_3^- in surface snow at Dome C to estimate the bulk fractionation constant ε (Table 1). Error bars are smaller than the symbols.

ACPD
9, 12559–12596, 2009

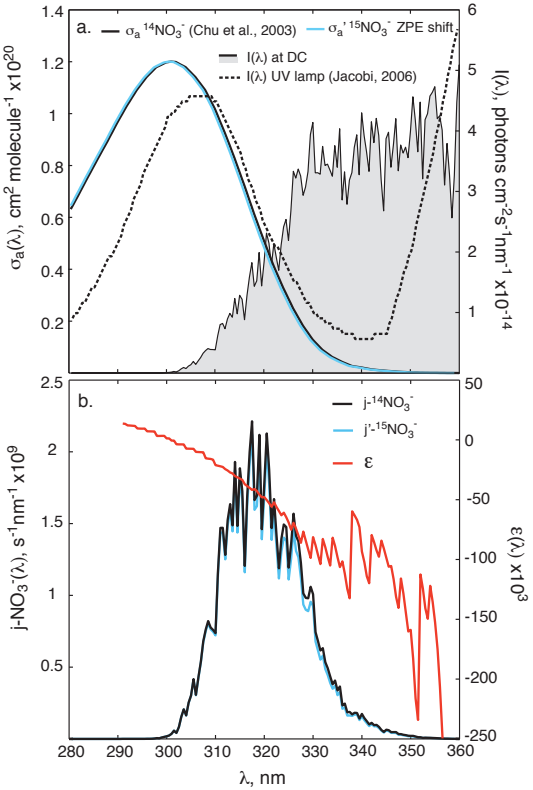

Fig. 5. Photoinduced fractionation effects (PHIFE) of $\delta^{15}N(NO_3^-)$ at Dome C: **(a)** UV absorption spectra of aqueous $^{14}NO_3^-$ (Chu and Anastasio, 2003) and $^{15}NO_3^-$ (estimated with ZPE shift) and modeled spectral actinic flux at DC on 15 January 2004 allow to calculate **(b)** photolysis rates for both NO_3^- isotopologues and the photolytic fractionation factor ε. The spectrum of the UV lamp used in lab experiments by Jacobi et al. (2006) is shown for comparison (a).

ACPD
9, 12559–12596, 2009

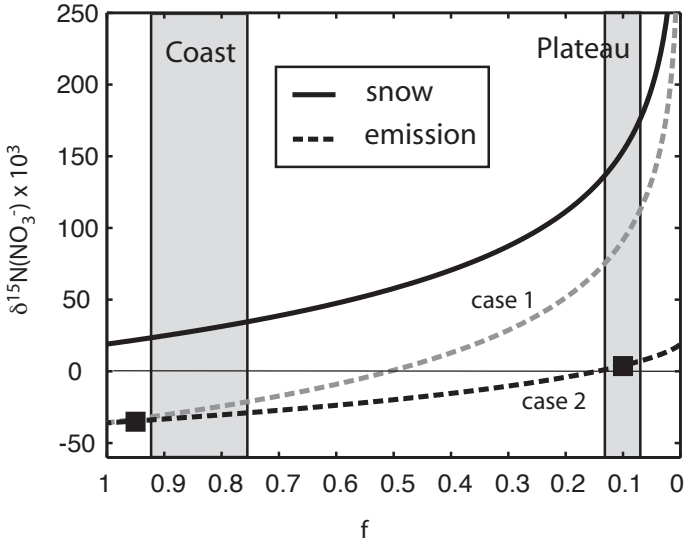

Fig. 6. Modeled $\delta^{15}N(NO_3^-)$ in snow and emissions against the remaining NO_3^- mass fraction in snow. Squares represent atmospheric NO_3^- measured at DC in October and December 2007. Expected NO_3^- losses in the study area (areas shaded in grey) are based on annual accumulation rate (Blunier et al., 2005; Dibb et al., 2007). Emission scenarios considered are immediate removal after release (case 1) and accumulation of emissions above the local snow surface, equivalent to the integration of all emissions from case 1 (case 2).

ACPD
9, 12559–12596, 2009